



The Study of High-Order Force on Electromagnetic Vibration of PMSMs

Jianfeng Hong^(✉), Shanming Wang, Yuguang Sun, and Haixiang Cao

Tsinghua University, Beijing 100084, China
hongjianfeng2009@126.com

Abstract. The influences of electromagnetic force with high order on electromagnetic vibration of permanent magnet motor are analyzed by using teeth chopping effect. First, the amplitudes, orders and frequencies of the electromagnetic forces are calculated by using the Maxwell stress tensor method. Then, the teeth chopping effect is introduced to describe the principle of low-mode vibration caused the high-order force. Next, the radial forces of three prototype motors are simulated and compared in detail, and the teeth chopping effect is validated by using the finite element method. Finally, the no-load electromagnetic vibration test is carried out on a 6p/36s permanent magnet motor, and test results are agreement with the simulation results. The results show that the high-order forces can cause the low-mode electromagnetic vibration with a non-negligible amplitude, and the research will provide the idea for the accurate vibration prediction and vibration reduction of the slotted permanent magnet motor.

Keywords: High-order force · Electromagnetic vibration · PM motor

1 Introduction

Permanent magnet synchronous machines (PMSM) had been widely used in industry as the driving element because of their good performance in power density and efficiency [1]. Recently, the vibration-noise indicator has become one of the key indicators to measure motor performance. The vibration and noise of the PM motor are investigated in many researchers [2–5]. The results show the low-order radial force can cause a significant vibration, and the order numbers of radial force are related to the pole and slot number of the motor.

The real slotted structure of the stator always be treated as the perfect ring in the analytical method to measure the vibration, and the high-order radial forces are always ignored when the vibration is calculated [6–8]. The study of high-order radial force on PM motor vibration is studied in [9, 10], and the breathing zeroth mode shape vibration in the PM machine is analyzed in [11, 12].

However, the study of the high-order radial force on motor vibration is not further explored and analyzed, and this paper focuses on the detailed motor vibration analysis excited by high-order radial force. This research will provide the idea for the accurate vibration prediction and vibration reduction of the slotted PM motor.

2 Teeth Chopping Effect

To explore the effect of high-order force on electromagnetic vibration in slotted PM motors, the teeth chopping effect [10] is introduced to describe the principle of the low-mode radial vibration excited by high-order radial force, as shown in Fig. 1, and it indicates the slot-number order force near the air-gap can induce a zeroth-mode vibration.

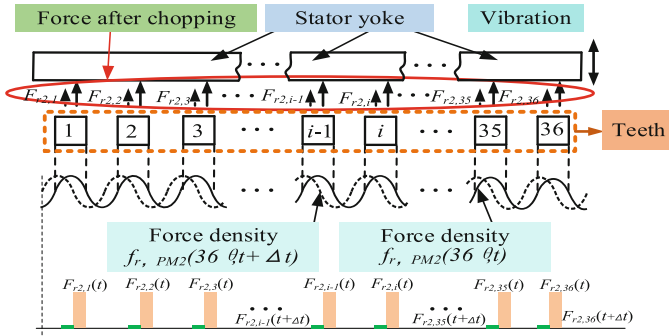


Fig. 1. Teeth chopping effect

3 Analysis of Exciting Force

The distributed radial force in the air-gap generated by PM magnetic field on no-load can be expressed by

$$f_{r,PM}(\theta, t) = \frac{B_{PM}^2(\theta, t)}{2\mu_0} \approx f_{r,PM1}(\theta, t) + f_{r,PM2}(\theta, t) \tag{1}$$

where

$$f_{r,PM1}(\theta, t) = \frac{1}{\mu_0} B_{PM1}(\theta, t) \cdot B_{PM2}(\theta, t) = \frac{\Lambda_0}{4\mu_0} \sum_{n_1} \sum_{n_2} \sum_k F_{n_1} F_{n_2} \Lambda_k \cdot \cos\{(n_1 \pm n_2)p\omega t - [(n_1 \pm n_2)p \pm kZ]\theta\} \tag{2}$$

$$f_{r,PM2}(\theta, t) = \frac{1}{2\mu_0} B_{PM1}^2(\theta, t) = \frac{1}{4\mu_0} \Lambda_0^2 \sum_{n_1} \sum_{n_2} F_{n_1} F_{n_2} \cdot \cos[(n_1 \pm n_2)p\omega t - (n_1 \pm n_2)p\theta] \tag{3}$$

Suppose $(n_1 \pm n_2)p = kZ$, and $k = 1$, k is preceded by a minus sign, it can be deduced as:

$$f_{r,PM1}(\theta, t)|_{r=0} = \frac{1}{\mu_0} B_{PM1}(\theta, t) \cdot B_{PM2}(\theta, t) = \frac{\Lambda_0}{4\mu_0} \Lambda_1 \cdot \sum_{n_1} \sum_{n_2} F_{n_1} F_{n_2} \cos\{(n_1 \pm n_2)p\omega t\} \tag{4}$$

This is the zeroth-order force density. When $k = 1$, and the positive sign is taken in front of k , the second slot-order force density at first slot frequency can be deduced:

$$f_{r,PM1}(\theta, t)|_{r=2Z} = \frac{\Lambda_0}{4\mu_0} \Lambda_2 \sum_{n_1} \sum_{n_2} F_{n_1} F_{n_2} \cdot \cos\{(n_1 \pm n_2)p\omega t + 2Z\theta\} \tag{5}$$

In fact, when $k = 3$, the second slot number order force density at slot frequency will also exist. When $k = 2$, the third slot-order force density will be deduced.

$$f_{r,PM1}(\theta, t)|_{r=3Z} = \frac{\Lambda_0}{4\mu_0} \Lambda_3 \sum_{n_1} \sum_{n_2} F_{n_1} F_{n_2} \cdot \cos\{(n_1 \pm n_2)p\omega t + 3Z\theta\} \quad (6)$$

where, the values of Λ_1 , Λ_2 and Λ_3 are related to the Carter factor.

Equation (3) shows that if $(n_1 \pm n_2)p = Z$, the slot number order force density at slot frequency dominates. The concentrated force obtained from Eq. (3) on i -th tooth is:

$$F_{r2,i}(t) = \frac{R_{si}L\Lambda_0^2}{2\mu_0} \sum_{n_1} \sum_{n_2} F_{n_1} F_{n_2} \frac{\sin[(n_1 \pm n_2)p\theta_b/2]}{(n_1 \pm n_2)p} \cos[(n_1 \pm n_2)p\omega t - (n_1 \pm n_2)p\frac{2\pi}{Z}i] \quad (7)$$

The concentrated force obtained from Eq. (4) on the i -th tooth is:

$$F_{r1,i}(t) = \frac{R_{si}L\theta_b\Lambda_0}{4\mu_0} \Lambda_1 \sum_{n_1} \sum_{n_2} F_{n_1} F_{n_2} \cos[(n_1 \pm n_2)p\omega t] \quad (8)$$

The concentrated force obtained from Eq. (5) on the i -th tooth is:

$$F_{r1,i}(t)|_{r=2Z} = \frac{R_{si}L\Lambda_0}{2\mu_0} \sum_{n_1} \sum_{n_2} F_{n_1} F_{n_2} \frac{\sin[Z\theta_b]}{2Z} (\Lambda_1 + \Lambda_3) \cos[(n_1 \pm n_2)p\omega t - 2(n_1 \pm n_2)p\frac{2\pi}{Z}i] \quad (9)$$

The concentrated force obtained from Eq. (6) on the i -th tooth is:

$$F_{r1,i}(t)|_{r=3Z} = \frac{R_{si}L\Lambda_0}{2\mu_0} \sum_{n_1} \sum_{n_2} F_{n_1} F_{n_2} \frac{\sin[3Z\theta_b/2]}{3Z} (\Lambda_1 + \Lambda_3) \cos[(n_1 \pm n_2)p\omega t - 3(n_1 \pm n_2)p\frac{2\pi}{Z}i] \quad (10)$$

As can be seen from the Eq. (7), (8), (9) and (10), the $F_{r2,i}$, $F_{r1,i}$, $F_{r1,i}|_{r=2Z}$ and $F_{r1,i}|_{r=3Z}$ can contribute to the 0-mode deformation and vibration. So, the 0-order force acting on the motor should be the resultant force of the Eq. (7), (8), (9) and (10). Therefore, the total slot-order frequency zero-order forces can be shown as:

$$F_{T,i} = F_{r2,i} + F_{r1,i} + F_{r1,i}|_{r=2Z} + F_{r1,i}|_{r=3Z} \quad (11)$$

As shown in (11), the total force consists of four items in turn: the force excited by the first slot-order force density, the force caused by zero-order force density, the force excited by the second slot-order force density and the force excited by the third slot-order force density. Furthermore, the values of these force densities are affected by the Carter factor. To explain it, three examples of different motors are analysed.

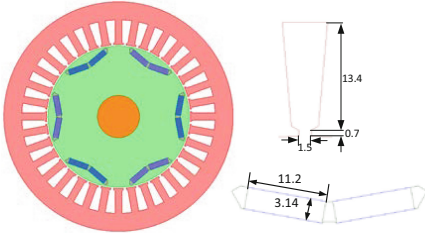


Fig. 2. FEM model

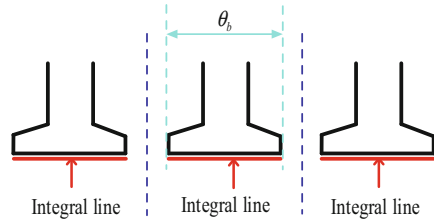


Fig. 3. The integral line

4 Simulation Results

4.1 6p/36s IPMSM (Type I)

The FEM model is built by Ansys Maxwell, as shown in Fig. 2. The specific parameters can be seen in [10].

As shown in Fig. 3, the radial force density is calculated by using Maxwell stress tensor method near the stator inner air-gap, and then the resultant forces of the tooth are calculated by integrating the force density. Considering the periodicity, twelve of the 36 resultant forces are shown in Fig. 4.

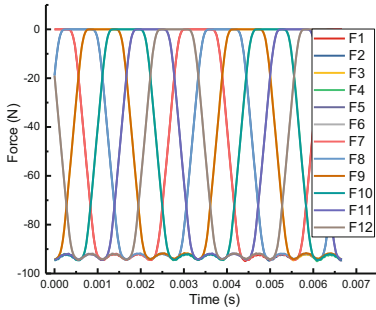


Fig. 4. The resultant forces of 12 tooth

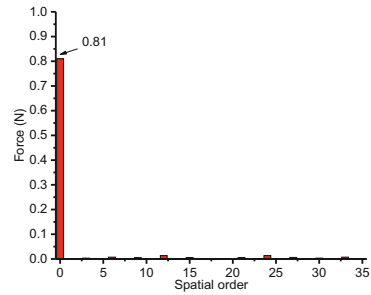


Fig. 5. The spatial order of force at slot frequency

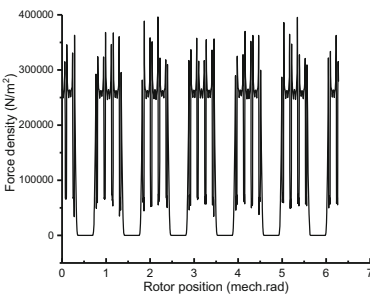


Fig. 6. Force in the air/iron interface

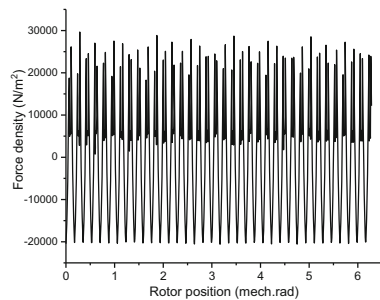


Fig. 7. Force density distribution at slot frequency

Thereafter, the temporal and spatial harmonics of the resultant forces are obtained using 2D FFT with the 36 resultant force waveforms. Figure 5 presents the spatial order of force at the slot frequency. As can be shown that the main spatial force harmonic is the zero-order force, and the value is 0.81 N.

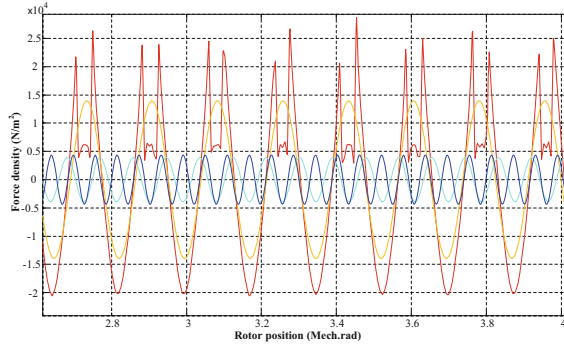


Fig. 8. FFT of force density at slot frequency

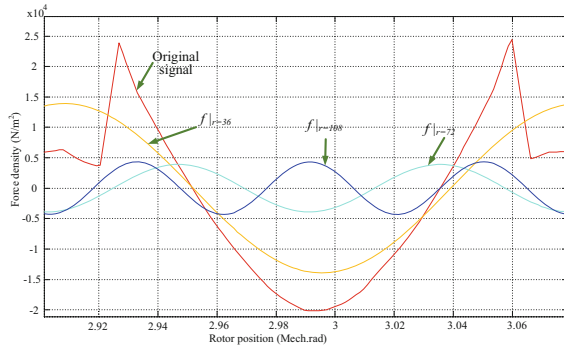


Fig. 9. Enlarged partial view of FFT

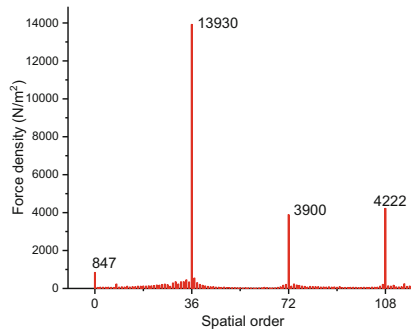


Fig. 10. The 36-order (temporal order) force harmonics

On the other hand, the spatial force harmonics of the resultant force on tooth can also be calculated using the formula. Firstly, the force density on the stator inner bore is obtained, its spatial distribution at one time step is shown in Fig. 6. Then, the temporal and spatial harmonics of the force density are calculated using 2D FFT. The 36-order force harmonics (which is related to the stator slot number) are shown in Fig. 6. Figure 7 presents the distributed slot-frequency radial force. Figure 8 is the FFT results of slot-frequency force, and Fig. 9 is the enlarged view of Fig. 8. The 36-(slot number) order force density harmonics are seen in Fig. 10.

In Fig. 10, the amplitude of the zero-order spatial force density is 847 N/m^2 . According to the (9), we can get that $F_{r1,i} = 0.28$. The maximum spatial force density harmonic is the 36-order force density harmonics, and its amplitude is 13930 N/m^2 . Similarly, the zero-order force integrated from the first slot-order force density is $F_{r2,i} = 1.11$. Then, the value of zero-order force caused by second-order force density is $F_{r1,i|r=72} = 0.252$, and the value of zero-order force caused by third-order force density is $F_{r1,i|r=108} = 0.18$. Special attention needs to be paid to the phase between different spatial orders, as can be shown from Fig. 9. Therefore, the total slot-order frequency zero-order force is equal to.

$$F_T = -F_{r1,i} - F_{r2,i} + F_{r1,i}|_{r=72} + F_{r1,i}|_{r=108} = -0.28 - 1.11 + 0.252 + 0.18 = -0.96\text{N}$$

and the magnitude is close to the resultant force 0.81 in Fig. 5.

4.2 6p/36s SPMSM (Type II)

The FEM model is built by Ansys Maxwell, as shown in Fig. 11. The specific parameters can be seen in [10].

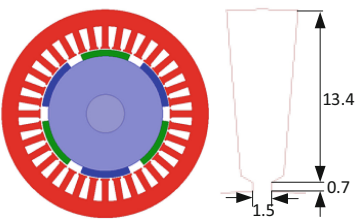


Fig. 11. FEM model

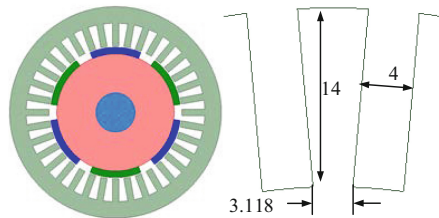


Fig. 12. FEM model

4.3 6p/36s SPMSM with Narrow Slot Width (Type III)

This FEM model of 6p/36s SPMSM only changes the slot width based on the Example 2, as shown in Fig. 12. Table 1 shows the slot-order frequency zero-order forces calculated by two methods under three motors. Comparing the total force by Method 1 and Method 2, the results are close.

Table 1. Simulation Results of three motors

	Type	I (N)	II (N)	III(N)
Method 1	Magnitude of Total force	0.81	1.61	2.85
	By zero-order force density	-0.28	0.45	0.607
	By first slot-order force density	-1.11	1.87	2.32
Method 2	By second slot-order force density	0.25	-0.35	-0.15
	By third slot-order force density	0.18	-0.21	-0.06
	Magnitude of Total force	0.96	1.76	2.72

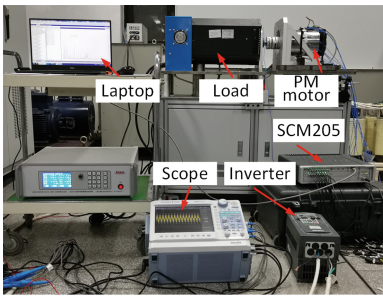


Fig. 13. Vibration test rig

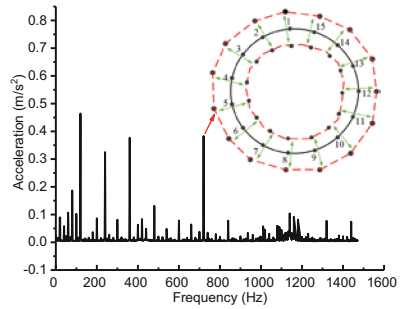


Fig. 14. Tested vibration acceleration when the motor runs at 900 r/min

5 Experiments

Figure 13 is the motor vibration test platform, and it includes the 6-pole/36-slot PM motor, SCM205 data acquisition, Inverter, Scope, Load and Laptop. Figure 14 presents the tested vibration acceleration when the motor runs at 1200 r/min with no-load. It can be seen that the peak frequency harmonics of the measured vibrations are the integer multiples of the product of the motor poles and rotor rotation frequency ($f = n/60$). The vibration mode shape shows a breathing shape at the frequency 720 Hz, which is the same as the analytical result.

6 Conclusion

In this paper, it can be conclude that: 1) The high-order air-gap radial force can induce the low-mode radial vibration; in the integer-slot PM motor, the high-order slot-number force is the dominant force to excite the vibration with 0th-mode, and the slot-order frequency zero-order forces obtained from the slot-number radial force occupy a large proportion; 2) If the proportion of zero-order force $F_{r1,i}$ obtained by the zero-order radial force is relatively small, the resultant force is basically equal to the force calculated by the slot-order air-gap radial force, and its contribution is independent of the load; the

values of different spatial order harmonics of radial force are related to Carter coefficient;
 3) In the design process of low vibration motor, the shape of the PM and stator tooth can be optimized.

Acknowledgments. This work was supported in part by the National Natural Science Funds of China under Grant 52007091.

References

1. Ma, W., Wang, D., Cheng, S., et al.: Common basic scientific problems and development of leading-edge technology of high performance motor system. *Proc. CSEE* **36**(8), 2025–2035 (2016). (in Chinese)
2. Yang, H., Chen, Y.: Influence of radial force harmonics with low mode number on electromagnetic vibration of PMSM. *IEEE Trans. Energy Conv.* **29**(1), 38–45 (2014)
3. Carraro, E., Bianchi, N., Zhang, S., et al.: Design and performance comparison of fractional slot concentrated winding spoke type synchronous motors with different slot-pole combinations. *IEEE Trans. Ind. Appl.* **54**(3), 2276–2284 (2018)
4. Sun, T., Kim, J., Lee, G., et al.: Effect of pole and slot combination on noise and vibration in permanent magnet synchronous motor. *IEEE Trans. Magn.* **47**(5), 1038–1041 (2011)
5. Kim, D., Park, M., Sim, J., et al.: Advanced method of selecting number of poles and slots for low-frequency vibration reduction of traction motor for elevator. *IEEE/ASME Trans. Mechatron.* **22**(4), 1554–1562 (2017)
6. Zhu, Z., Xia, Z., Wu, L., et al.: Analytical modeling and finite-element computation of radial vibration force in fractional-slot permanent-magnet brushless machines. *IEEE Trans. Ind. Appl.* **46**(5), 1908–1918 (2010)
7. Valavi, M., Nysveen, A., et al.: Influence of pole and slot combinations on magnetic forces and vibration in low-speed PM wind generators. *IEEE Trans. Magn.* **50**(5), 8700111 (2014)
8. Chen, Y., Zhu, Z., Howe, D.: Vibration of PM brushless machines having a fractional number of slots per pole. *IEEE Trans. Magn.* **42**(10), 3395–3397 (2006)
9. Fang, H., Li, D., Qu, R., et al.: Modulation effect of slotted structure on vibration response in electrical machines. *IEEE Trans. Ind. Electron.* **66**(4), 2998–3007 (2019)
10. Wang, S., Hong, J., Sun, Y., et al.: Analysis of zeroth mode slot frequency vibration of integer slot permanent magnet synchronous motors. *IEEE Trans. Ind. Electron.* **67**(4), 2954–2964 (2019)
11. Huang, S., Aydin, M., Lipo, T.: Electromagnetic vibration and noise assessment for surface mounted PM machines. In: *Power Engineering Society Summer Meeting*, Vancouver, Canada (2001)
12. Li, X., Huang, S., Li, L.: Calculation and analysis of vehicle vibration and noise of permanent magnet synchronous motor applied in electric vehicle. *Electric Mach. Control* **17**(8), 37–42 (2013). (in Chinese)